ANALYSIS OF RESIDUAL STRESS IN FIBRE-REINFORCED POLYMER COMPOSITES

Liguo Zhao*, Nick A Warrior, Andrew C Long****
***University of Portsmouth, **University of Nottingham**

Keywords: *Residual stress, Thermo-viscoelastic, Finite element, Failure envelope.*

Abstract

Process-induced residual stress in fibre-reinforced thermoset polymer-matrix composites was analysed using a unit cell model and the finite element method, with the consideration of chemical shrinkage of the epoxy resin and thermal cooling contraction of the whole fibre and resin system. The constitutive behaviour of the epoxy matrix was described by a cure and temperature dependent viscoelastic material model. Calculated residual stress shows strong dependency on the fibre volume fraction and fibre packing. The effect of residual stress on damage and failure of the model was also studied using the maximum stress failure criterion combined with a post-failure stiffness reduction technique. Both initial and final failure envelopes, predicted for biaxial normal (longitudinal and transverse) loading, were shown to be shifted and contracted by the inclusion of residual stress.

1 Introduction

Process-induced residual stress in polymer-matrix composites is a direct consequence of the chemical shrinkage of the matrix during polymerisation and the mismatch of thermal contraction between the fibre and the matrix during cooling. The formation of residual stresses can have significant effects on the mechanical performance of composite structures by causing warpage [1] or initiating pre-load damage such as interface debonding and matrix microcracking [2, 3]. Both warpage and initial damage can reduce the stiffness and the strength of the material, as well as acting as sites for nucleation of macrocracks and environmental degradation.

For thermoset polymer composites, a typical curing process consists of two steps: curing at a constant elevated temperature and thermal cooling from the curing temperature to room temperature. During curing, the polymer shrinks as a result of the purely chemical reaction (polymerisation) and its material characteristics change dramatically through the transition from a liquid state to a solid state while the reinforcement remains unchanged [4, 5]. For thermal cooling, both polymer and reinforcement contract but by different amounts and in addition the polymer may change its stiffness significantly. Therefore, the build-up of residual stress over time is governed by the change of volume and material properties during the complete cure process.

Effects of residual stress on mechanical behaviour of the composite materials have been studied primarily by analytical methods. Nimmer [6] and Wisnom [7] showed that the presence of compressive residual stress at the interface of fibre and matrix is beneficial for the transverse behaviour of a composite with low interfacial strength. It was also shown that residual stress can result in changing and movement of the yielding surfaces for metal matrix composites [8]. For polymer-matrix composites, process-induced residual stress may introduce contraction and shifting of biaxial failure envelopes for transverse loading [9].

Residual stress is one of the major concerns in the manufacturing of polymer-matrix composites, especially the effects of residual stress on damage and failure behaviour. In the present work, finite element analysis was used to study residual stress and its effect on damage and failure of fibre-reinforced thermoset polymer matrix composites using a micromechanical unit cell model. The residual stress introduced during curing was determined by considering both chemical shrinkage of resin and thermal cooling contraction of fibre and resin. A cure and temperature dependent viscoelastic material model was adopted to describe the constitutive relationship of the polymer matrix. Effects of fibre volume fraction and packing on residual stress were investigated. In addition, effects of residual stress on damage and failure of the unit cell subjected to mechanical loading after curing were predicted using the maximum stress failure criterion and a post-failure stiffness reduction technique.

2 Material

2.1 Cure Kinetics

Thermoset resin undergoes chemical reactions during the curing process at an elevated temperature. Curing of a resin occurs over time and the degree of cure depends on the temperature history. The chemical kinetics of thermoset resin defines the dependency of the degree of cure on temperature history. In order to capture the conversion-dependent material properties, the resin cure kinetics need to be characterized accurately. For epoxy resins, the autocatalytic model has been used widely to describe cure kinetics and this is also adopted here. The model can be expressed as follows [10]

$$\frac{d\alpha}{dt} = (K_1 + K_2\alpha^{n_1})(1-\alpha)^{n_2}\,, \tag{1}$$

$$K_1 = K_{01}\exp\left(\frac{-E_{01}}{RT}\right),$$
$$K_2 = K_{02}\exp\left(\frac{-E_{02}}{RT}\right), \tag{2}$$

where α is the degree of cure, t the time, K_1 and K_2 the rate constants, n_1 and n_2 the exponents, K_{01} and K_{02} the temperature-independent factors, E_{01} and E_{02} the activation energies, and R and T the universe gas constant and the temperature, respectively. The values of the parameters are given in Eom et al. [10]. As shown in Eom et al. [10], the predicted degree of cure from equations (1) and (2) agrees with the experimental measurements very well for cure temperatures between 150°C and 170°C.

2.2 Viscoelastic Model

As shown in Xia et al. [11], viscoelastic material behaviour for epoxy resin can be well described by a combination of Kelvin elements connected in series in a uniaxial representation. As a result, viscous strain rate can be obtained as the sum of the strain rate of each Kelvin element, i.e.,

$$\dot{c}_{ij} = \sum_{m=1}^{n}\dot{c}_{ij}^{m} = \sum_{m=1}^{n}\left(\frac{S_{ijkl}}{E_m\tau_m}\sigma_{kl} - \frac{1}{\tau_m}c_{ij}^{m}\right), \tag{3}$$

where S_{ijkl} is the compliance components and $\tau_m = \eta_m/E_m$ ($m = 1, 2, \ldots, n$) denotes the retardation time with E_m being the spring stiffness and η_m being the dashpot viscosity for the m-th Kelvin element, respectively.

The retardation time τ_m in equation (3) determines a time duration after which the contribution from the individual Kelvin element becomes negligible. Therefore, the number of Kelvin elements adopted in the constitutive equation depends on the required time range. For simplicity, a time scale factor β was introduced in Xia et al. [11] and it was assumed that

$$\tau_m = (\beta)^{m-1}\tau_1\,. \tag{4}$$

The description of the nonlinear behaviour in the above model was achieved in Xia et al. [11] by letting E_m be a function of the current equivalent stress, thus,

$$E_m = E_1(\sigma_{eq})$$
$$= 1.055\times10^5\exp\left(-\frac{\sigma_{eq} - 22.764}{18.0}\right). \tag{5}$$

For epoxy resin, it was shown in Xia et al. [12] that the material shows different behaviour in uniaxial tension and compression. To account for this, the equivalent stress in equation (5) was defined as

$$\sigma_{eq} = \frac{(R-1)I_1 + \sqrt{(R-1)^2 I_1^2 + 12RJ_2}}{2R}\,, \tag{6}$$

where $I_1 = \sigma_1 + \sigma_2 + \sigma_3$ is the first invariant of the stress tensor, $J_2 = S_{ij}S_{ij} / 2$ is the second invariant of the deviatoric stress S_{ij}, and R is the ratio of the tensile to compressive “yield stress”.

2.3 Cure and Temperature Dependent Material Properties

The composite constituents considered here are glass fibre and epoxy resin. The properties of glass fibre are assumed to remain constant and independent of temperature, with the Young’s modulus E = 72.5 GPa, the Poisson’s ratio ν = 0.22 and the coefficient of thermal expansion χ = 5.0×10^{-6} / °C [13].

For epoxy resin, the Young's modulus is a function of the temperature T and the degree of cure α, which is expressed as [14]

$$E(T,\alpha) = \alpha \frac{E_0}{\cosh(aT)^b}, \qquad (7)$$

where E_0 is the Young's modulus for fully cured resin at room temperature, a and b are constants. The function (7) is also applied for the spring stiffness E_m of each Kelvin element to simulate the dependency of spring stiffness on the temperature and the degree of cure, i.e.,

$$E_m = \alpha \frac{E_1(\sigma_{eq})}{\cosh(aT)^b}. \qquad (8)$$

The thermal expansion coefficient χ of the epoxy resin is expressed as a linear function of the temperature, with $\chi = 63\times10^{-6}$ / °C for 23°C and $\chi = 139\times10^{-6}$ / °C for 110°C [13].

In addition, the Poisson's ratio for epoxy resin is taken to be constant and assumed to be independent of degree of cure and temperature. Values of the material properties and the model parameters required by equations (3) to (8) are all given in [11] and [14].

3 Analysis of Residual Stress

Residual stress caused by constrained shrinkage and thermal cooling contraction of the resin can be expressed as

$$d\sigma_{ij} = C_{ijkl}\left\{d\varepsilon_{ij} - dc_{ij} - \delta_{ij}ds - \delta_{ij}\alpha(T)dT\right\}, \qquad (9)$$

where $d\sigma_{ij}$ are the stress increments, $d\varepsilon_{ij}$ the total strain increments, dc_{ij} the viscous strain increments, ds the shrinkage strain increment, $\alpha(T)$ the thermal expansion coefficient, δ_{ij} the Kronecker delta, dT the temperature change, and C_{ijkl} the stiffness components.related to the Young's modulus E and the Poisson's ratio ν of the material.

In Equation (9), the viscous strain can be obtained from the viscoelstic model in Section 2.2 and the thermal strain can be obtained from the assigned thermal expansion coefficients and temperature history. The chemical shrinkage strain needs to be determined from the volumetric shrinkage of the resin associated with the reaction process. For a given incremental change in the degree of cure during reaction $d\alpha$, the associated change in specific volume of the resin dV can be expressed as [15, 16],

$$dV = d\alpha V_{sh}, \qquad (10)$$

where V_{sk} is the total volume change in the resin at the end of cure. The isotropic resin shrinkage strain of a unit volume element of resin, resulting from an incremental volume resin shrinkage, is then given by [15, 16]

$$ds = \sqrt[3]{1 + dV} - 1. \qquad (11)$$

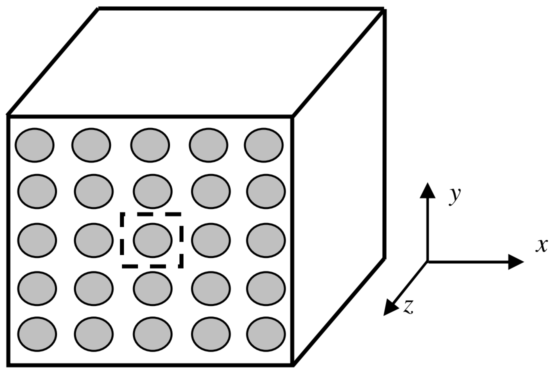

Fig.1 Illustration of the unit cell (enclosed by dashed lines) for square fibre arrays.

4 Finite Element Model

In composites, the actual fibre distribution is quite random over a cross section. For simplicity, most micromechanical models assume a periodic arrangement of fibres for which a unit cell can be isolated. The unit cell has the same elastic constants and fibre volume fraction as the composite. The periodic fibre sequences commonly used are the square, square-diagonal and hexagonal arrays. In this work, the square array as shown in Fig.1 is primarily considered in the finite element analysis and the matrix is assumed to be perfectly bonded to the fibres throughout the analysis. In addition, the square-diagonal and hexagonal arrays were also considered in order to study the effect of fibre packing on the generation of residual stress.

Due to the symmetry only a quarter of the unit cell (Fig.2) is considered. Boundary conditions used for the quarter unit-cell model are summarized as follows

$u = 0$ at face ABFE, $v = 0$ at face BCGF and $w = 0$ at face ABCD, (12) Equal u for face DCGH, equal v for face ADHE and equal w for face EFGH, (13)

where u, v and w stand for the displacements in the x, y and z directions, respectively

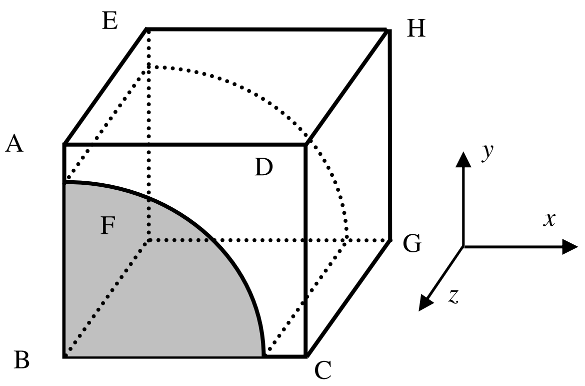

Fig.2 A quarter of unit cell.

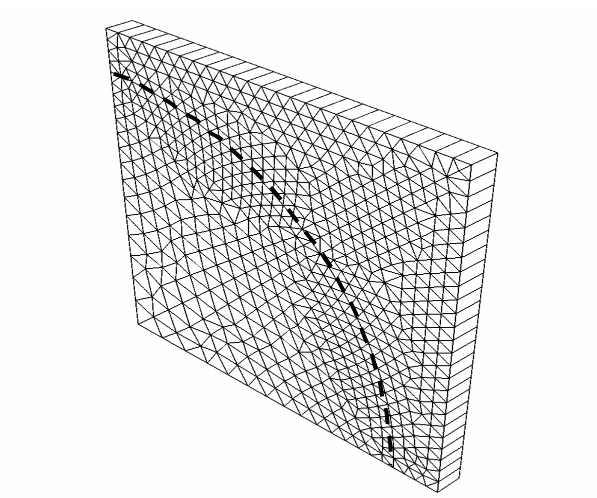

Fig.3 Finite element mesh for a quarter of unit cell for square packing (dashed line indicates the interface).

The mesh generated for the quarter model is shown in Fig.3 where the fibre volume fraction is taken to be 60% and 15-noded three-dimensional wedge elements are used. The number of elements is approximately 1,300 for the quarter unit cell model. The average element size within the fine mesh region is around 4% of the fibre radius. Note that the mesh shown in Fig.3 only has one layer of elements in the fibre direction. Analyses have been carried out for meshes with multi-layers (up to twenty) elements in the fibre direction, and the same strain and stress fields (independent of the z coordinate) were obtained. Hence, for computational efficiency, the mesh with only one-layer elements in the fibre direction (see Fig.3) was considered throughout this work. Furthermore, mesh sensitivity analyses have shown that the mesh shown in Fig.3 is fine enough to produce accurate results compared to a doubly refined mesh, with a difference within 0.3% in terms of residual stress and failure load level.

5 Damage and Failure Prediction

As shown in Fig.1, the unit cell model consists of fibre reinforcement and resin matrix. Depending on the failure mechanism, the following criteria for damage onset prediction were used.

For transverse failure, damage tends to occur within the resin matrix and is related to the stress state within the (x, y) plane. In this case, failure is predicted from the maximum principal stress criterion in the (x, y) plane, i.e.

$$\sigma_{\max}^{(x,y)} \geq \sigma_u^t \text{ or } \sigma_{\min}^{(x,y)} \leq \sigma_u^c \tag{14}$$

where $\sigma_{\max}^{(x,y)}$ and $\sigma_{\min}^{(x,y)}$ are the maximum and minimum principal stresses in the (x, y) plane and σ_u^t and σ_u^c are the tensile and compressive strengths of the resin, respectively.

For longitudinal failure, damage might occur in both the fibre and the resin. Obviously, longitudinal failure is due to the normal stress in the fibre direction and the failure criterion can be expressed as

$$\sigma_{zz} \geq \sigma_u^t \text{ or } \sigma_{zz} \leq \sigma_u^c \tag{15}$$

where σ_{zz} is the normal stress in the z-direction (fibre-direction) and σ_u^t and σ_u^c are the tensile and compressive strengths of the fibre or the resin, respectively.

Material strengths used for failure prediction are taken from Soden et al. [17] with tensile strength of 2150MPa and compressive strength of 1450MPa for the glass fibre and tensile strength of 80MPa and compressive strength of 120MPa for the epoxy resin

In simulating material damage, it is common practice to reduce the stiffness (or stiffness in a certain direction) to a near zero value following the onset of damage. Selective and non-selective stiffness reduction schemes are often used. Selective schemes are typically applied for composites where the load-carrying nature is dependent on the damage orientation [18]. In the present study, under normal loading, damage is distinguished by the transverse and longitudinal failure for matrix and thus a selective scheme is used. Specifically, for transverse failure only the modulus in the transverse direction was reduced to a near zero value (0.01 times the original value) after damage onset, while for longitudinal failure, only the modulus in the longitudinal direction was reduced (also 0.01 times the original value).

The stiffness degradation scheme, together with the residual stress analysis from equation (9), was programmed into a user-defined material subroutine (UMAT) interfaced with the commercial finite element code ABAQUS standard [19]. During the analysis, the stress level was calculated at the Gauss integration points for each time increment and examined for damage detection using the above failure criteria. Once the failure criterion was satisfied, the stiffness reduction was applied for further analysis until final failure of the model.

6 Results and Discussion

6.1 Residual Stress

The cure process considered here has two stages: curing at 150°C for 3 hours and thermal cooling from 150°C to 23°C (room temperature) at a cooling rate of 2°C/min. Therefore finite element analysis was performed in two discrete steps, where step one is the chemical shrinkage stress analysis at 150°C and step two is the thermal cooling stress analysis from 150°C to 23°C. For the epoxy resin considered here, the total volume shrinkage V_{sh} was chosen to be 3% [20-22], which corresponds to a shrinkage strain of 0.99% (about 1%).

A contour plot of the maximum principal residual stress is shown in Fig.4 for square fibre packing with a fibre volume fraction of 60%. It can be seen that, as expected, the resin experiences a tensile maximum principal residual stress while the fibre has a compressive maximum principal residual stress. The greatest value (48.8MPa) occurs in the central region (at θ = 45°) of the fibre-matrix interface of the quarter unit-cell model, within the resin. According to the maximum stress failure criterion, the residual stress can introduce resin failure along the interface of the fibre and the resin, which agrees with the experimental observation of interface microcracking shown in Gentz *et al.* [2, 3].

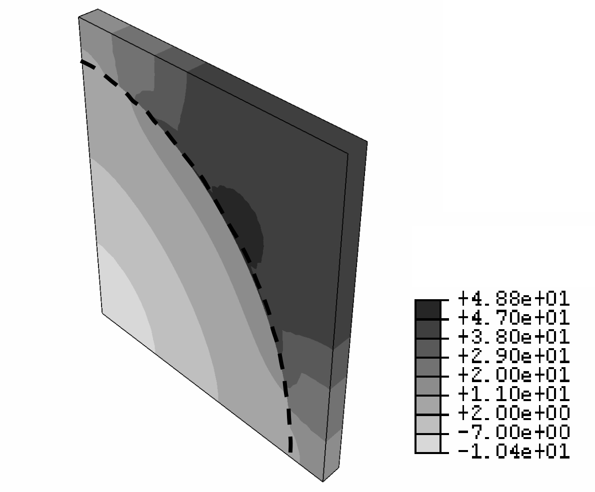

Fig.4 Contour plot of the maximum principal residual stress (MPa) for V_f = 60%.

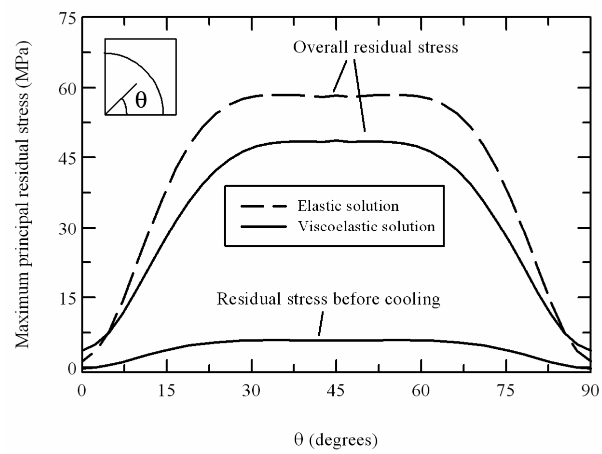

Fig.5 Distribution of the maximum principal residual stress in the resin along the fibre/matrix interface for V_f = 60%.

The distribution of the maximum principal residual stress in the resin along the interface is presented in Fig.5, where the elastic solution and the chemical shrinkage contribution are also included. Compared to the purely elastic solution, a reduction in residual stress was predicted due to the stress-relaxation caused by the viscoelastic behaviour of the epoxy matrix. Also the results show that the chemical shrinkage of resin makes only a relatively small contribution to the overall residual stress due to the relatively low modulus at the high cure temperature (150°C). At the central position in the interface of the quarter unit cell (θ = 45°), the maximum principal residual stress due to chemical shrinkage has a value of 5.9MPa, about 12% of the overall maximum principal residual stress 48.8MPa. This indicates that the curing shrinkage still makes a reasonable contribution to the overall residual stress, and should be included for stress analysis in polymer composites.

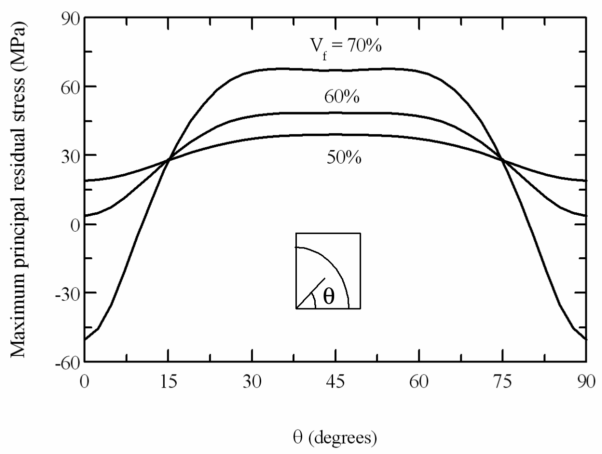

Fig.6 Distribution of the maximum principal residual stress in the resin along the fibre/matrix interface for three different fibre volume fractions.

The effects of fibre volume fraction on process-induced residual stress were studied for square packing arrangement. Fig.6 shows the maximum principal residual stress in the resin along the fibre-matrix interface for three different volume fractions, i.e., V_f = 50%, 60% and 70%, respectively. For all three volume fractions, the distribution of maximum principal residual stress follows a similar pattern, with the greatest value at θ = 45° and the lowest values at θ = 0° and 90°. The magnitude of residual stress was seen to increase with the increase in fibre content, since higher fibre content tends to prevent free shrinkage of the resin more significantly and causes increased residual stress. With the increase of fibre volume fraction, the maximum principal residual stress always remains tensile at θ = 45°. However, at θ = 0° and 90°, the maximum principal residual stress tends to become compressive with the increase of fibre volume fraction. For V_f = 70%, it is noticed that a compressive maximum principal residual stress, up to −50.2MPa, was developed at θ = 0° and 90°. Increased tensile residual stress at θ = 45° might facilitate crack initiation or interface debonding in these areas, while developed compressive residual stress at θ = 0° and 90° might be beneficial in preventing interface debonding in those areas [6, 7].

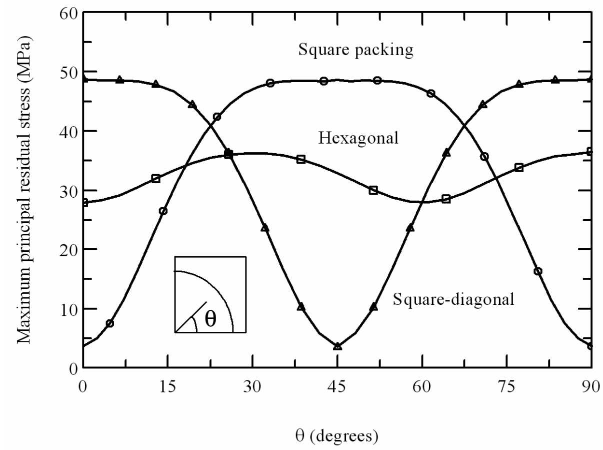

Fig.7 Distribution of the maximum principal residual stress in the resin along the fibre/matrix interface for three different fibre packing (fibre volume fraction V_f = 60%).

In addition to the square packing, hexagonal and square-diagonal packing were also considered to study the effects of fibre packing on residual stress (fibre volume fraction was 60% for both packing arrangements). Distributions of the maximum principal residual stress of the resin along the fibre/matrix interface are presented in Fig.7 for the three different fibre-packing arrangements. The magnitude of residual stress depends on the fibre arrays, with higher values for square and square-diagonal packing and lower values for hexagonal packing. The magnitude of maximum principal residual stress for hexagonal packing is about 36.8MPa at θ = 45°, about 25% lower than those seen in square and square diagonal packing. This may be as a result of the more uniform distribution of resin as seen in hexagonal packing.

6.2 Effects of Residual Stress on Failure Envelopes

To study the influence of residual stress on the response of the unit cell model, the damage onset and final failure were examined under mechanical loading for a square packing model with a fibre volume fraction of 60%. After curing and thermal cooling analysis, distributed normal traction was applied to the model surfaces. At each time increment of the analysis, the initiation and evolution of damage are monitored using the maximum stress failure criterion and stiffness reduction technique described in Section 5.

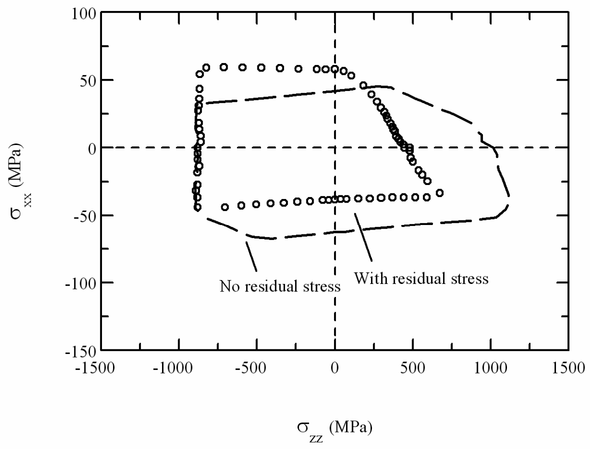

Fig.8 Effect of residual stress on initial failure envelopes for biaxial longitudinal and transverse normal loading.

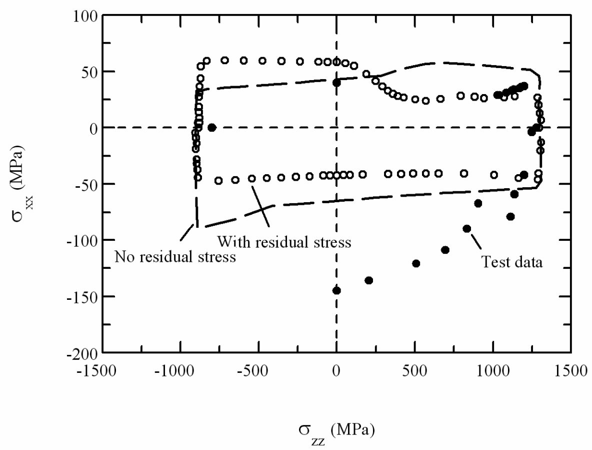

Fig.9 Effect of residual stress on final failure envelopes for biaxial longitudinal and transverse normal loading.

Under biaxial longitudinal (z-direction) and transverse (x-direction) normal loading, failure envelopes were constructed by considering different biaxial load ratios and the results are shown in Fig.8 and Fig.9 for initial and final failures, respectively. Failure envelopes for no residual stress, as well as the test data of final failure for unidirectional E-glass/epoxy composites from Soden et al. [23], are also included for comparison. Initial failure level corresponds to the onset of damage. With further increase of load after damage onset, damage develops from the location of onset and spreads over the unit cell. Final failure occurs when the damage spreads across the section normal to the loading direction which makes the unit cell unable to carry any further load. From Fig.8 and Fig.9, it can be seen that by considering the residual stress, both initial and final failure envelopes are shifted and contracted when compared to those derived by excluding residual stress. A similar shifting effect of residual stress on failure envelopes was also shown in Zhao et al. [9] for transverse biaxial normal loading. Also, Aghdam and Khojeh [8] showed that residual stress caused a shifting of initial yield surfaces for unidirectional fibre-reinforced metal-matrix composites under transverse loading. By comparing Fig.8 and Fig.9, it can be seen that initial and final failure envelopes are very different in the regions with tensile longitudinal loading, since the initial failure is mainly transverse and occurs within the matrix, which is much earlier than the final matrix or fibre failure. In the regions with compressive longitudinal loading, the initial and final failure envelopes are comparable due to the rapid spread of damage over the unit cell after the damage onset

From the failure envelopes in Fig.9, residual stress is shown to have little effect on the load levels for longitudinal final failure due to the high fibre strengths (see the two straight edges on the left and the right), but greatly affects the transverse failure behaviour due to the relatively low resin strengths. In the transverse failure region, residual stress is mainly detrimental for transverse compression by causing earlier compressive failure. For transverse tension, residual stress has a complex effect depending on the load ratios. Residual stress is beneficial for load ratio $-14.0 < R_{LT} < 4.0$ and detrimental for $4.0 < R_{LT} < 48.0$ (R_{LT} is the ratio of longitudinal load to transverse load).

Experimental data in Fig.9 follow the predictions in the tension-tension region, but show a big discrepancy in the tension-compression region. There are four aspects which might contribute to the discrepancy. Firstly, test data in Soden et al. [23] were taken from the biaxial tests performed by Al-Khalil et al. [24] on nearly unidirectional ±85° E-glass/MY750-epoxy tubes (with a fibre volume fraction of approximately 60%), which are, strictly speaking, bi-directional composites. Therefore, the tests could overestimate the transverse compressive strength due to the additional contributions from the fibres present in the transverse direction. Secondly, the curing procedure for the tested tubes was different, with 2 hours at 90°C followed by 1.5 hours at 130°C and 2 hours at 150°C [23], which might introduce different residual stress states in the tested tubes and affect their failure behaviour, particularly for transverse loading situations. Thirdly, the stress-based criterion for compressive damage prediction in the matrix resin used in this work might underestimate the failure level, since the test curve for compressive stress and strain shows a softening behaviour [12]. This means that compressive strength does not reflect the final failure correctly under compressive loading. Other failure criteria, such as a strain based failure criterion, may be more appropriate for detection of compressive failure in the resin matrix. Finally, non-ideal fibre distribution and concentration in real composites could also make contributions to this difference [25].

7 Conclusions

A thermoviscoelastic micromechanical model and the finite element method have been used to study process-induced residual stress in unidirectional fibre-reinforced polymer-matrix composites. Viscoelastic behaviour was assigned to the epoxy matrix with cure and temperature dependent material properties. From a three-dimensional unit cell, residual stress was computed by considering the chemical shrinkage of the epoxy resin and the thermal cooling contraction of the whole fibre and resin system.

Computed residual stress shows strong dependency on the fibre volume fraction and fibre packing. A higher fibre volume fraction will result in much greater residual stress levels due to stronger fibre constraints on the matrix contraction. Fibre-packing studies suggest that evenly distributed fibres, as in hexagonal packing, could reduce the magnitude of residual stress by weakening the overall fibre constraints.

Using the maximum stress failure criterion, effects of residual stress were addressed on failure envelopes. The inclusion of residual stress results in contraction and movement of both the initial and final failure envelopes predicted for biaxial normal (longitudinal and transverse) loading. For final failure, residual stress shows little effect on the load levels for fibre-dominated longitudinal failure, but greatly affects the load levels for matrix-dominated transverse failure.

Acknowledgement

This work is funded by the UK Engineering and Physical Sciences Research Council (EPSRC) through the Nottingham Innovative Manufacturing Research Centre (NIMRC).

References

[1] Dannenberg H. “Determination of stresses in cured epoxy resins”. *SPE Journal July*, pp 669-675, 1965.

[2] Gentz M., Armentrout D., Rupnowski P., Kumosa L., Shin E., Sutter J.K. and Kumosa M. “In-pane shear testing of medium and high modulus woven graphite fiber reinforced/polyimide composites”. *Composites Science and Technology*, Vol. 64, pp 203-220, 2004.

[3] Gentz M., Benedikt B., Sutter J.K. and Kumosa M. “Residual stress in unidirectional graphite fiber/polyimide composites as a function of aging”. *Composites Science and Technology*, Vol. 64, pp 1671-1677, 2004.

[4] Lange J., Toll S. and Månson J-A.E. “Residual stress build-up in thermoset films cured above their ultimate glass transition temperature”. *Polymer*, Vol. 36, pp 3135-3141, 1995.

[5] Flores F., Gillespie J.W. and Bogetti T.A. “Experimental investigation of the cure-dependent response of vinyl ester resin”. *Polymer Engineering and Science*, Vol. 42, pp 582-590, 2002.

[6] Nimmer R.P. “Fibre-matrix interface effect in presence of thermally induced residual stresses”. *Journal of Composites Technology and Research*, Vol. 12, pp 65-75, 1990.

[7] Wisnom M.R. “Factors affecting the transverse tensile strength of unidirectional continuous Silicon Carbide fibre reinforced 6061 Aluminium”. *Journal of Composite Materials*, Vol. 24, pp 707-726, 1990.

[8] Aghdam M.M., Smith D.J. and Pavier M.J. “Finite element micromechanical modelling of yield and collapse behaviour of metal matrix composites”. *Journal of the Mechanics and Physics of Solids*, Vol. 48, pp 499-528, 2000.

[9] Zhao L.G., Warrior N.A. and Long A.C. “A micromechanical study of residual stress and its effect on transverse failure in polymer-matrix composites”. *International Journal of Solids and Structures*, Vol. 43, pp 5449-5467, 2006.

[10] Eom Y., Boogh L. and Michaud V. “Time-cure-temperature superposition for the prediction of instantaneous viscoelastic properties during cure”. *Polymer Engineering and Science*, Vol. 40, pp 1281-1292, 2000.

[11] Xia Z., Hu Y. and Ellyin F. “Deformation behaviour of an epoxy resin subject to multiaxial loadings. Part II: constitutive modeling and predictions”. *Polymer Engineering and Science*, Vol. 43, pp 734-748, 2003.

[12] Xia Z., Hu Y. and Ellyin F. “Deformation behaviour of an epoxy resin subject to multiaxial loadings. Part

I: experimental investigations". *Polymer Engineering and Science*, Vol. 43, pp 721-733, 2003.

[13] Zhang Y., Xia Z. and Ellyin F. "Evolution and influence of residual stress/strains of fiber reinforced laminates". *Composites Science and Technology*, Vol. 64, pp 1613-1621, 2004.

[14] Ruiz E. and Trochu F. "Numerical analysis of cure temperature and internal stresses in thin and thick RTM parts". *Composites: Part A*, Vol. 36, pp 806-826, 2005.

[15] Bogetti T. and Jr. Gillespie J.W. "Process-induced stress and deformation in thick-section thermoset composite laminates". *Journal of Composite Materials*, Vol. 26, pp 626-660, 1992.

[16] Huang X., Jr. Gillespie J.W. and Bogetti, T. "Process induced stress fro woven fabric thick section composite structures". *Composites Structures*, Vol. 49, pp 303-312, 2000.

[17] Soden P.D., Hinton M.J. and Kaddour, A.S. "Lamina properties, lay-up configurations and loading conditions for a range of fibre-reinforced composite laminates". *Composites Science and Technology*, Vol. 58, pp 1011-1022, 1998.

[18] Blackketter D.M., Walrath D.E. and Hansen, A.C. "Modeling damage in a plain weave fabric-reinforced composite material". *Journal of Composite Technology Research,* Vol. 15], pp 136-142, 1993.

[19] ABAQUS 6.5, Hibbitt, Karlsson and Sorensen Inc, Providence, R.I., USA, 2005.

[20] Russell J.D. "Cure shrinkage of thermoset composites". *SAMPE Quarterly*, Vol. January, pp 28-33, 1993..

[21] Oota K. and Saka M. "Cure shrinkage analysis of epoxy moulding compound". *Polymer Engineering and Science*, Vol. 41, pp 1373-1379, 2001.

[22] Li C., Potter K., Wisnom M.R. and Stringer G. "In-situ measurement of chemical shrinkage of MY750 epoxy resin by a novel gravimetric method". *Composites Science and Technology*, Vol. 64: pp 55-64, 2004.

[23] Soden P.D., Hinton M.J. and Kaddour A.S. "Biaxial test results for strength and deformation of a range of E-glass and carbon fibre reinforced composite laminates: failure exercise benchmark data". Composites Science and Technology, Vol. 62, pp 1489-1514, 2002.

[24] Al-Khalil M.F.S., Soden P.D., Kitching R. and Hinton M.J. "The effects of radial stress on the strength of thin walled filament wound GRP composite pressure cylinders". *International Journal of Mechanical Science*, Vol. 38, pp 97-120, 1996.

[25] Bulsara V.N., Talreja R. and Qu J. "Damage initiation under transverse loading of unidirectional composites with arbitrarily distributed fibers". *Composites Science and Technology*, Vol. 59, pp 673-682, 1999.